Unique Structural Characteristics of Graft-Type Proton Exchange Membranes using SANS Partial Scattering Function Analysis

Yue Zhao,[1,*] Kimio Yoshimura,[1] Shinichi Sawada,[1] Toshinori Motegi,[1] Akihiro Hiroki,[1]

Aurel Radulescu,[2] Yasunari Maekawa[1,*]

[1]*Department of Advanced Functional Materials Research, Takasaki Advanced Radiation Research Institute, National Institutes for Quantum Science and Technology (QST), Watanuki-machi 1233, Takasaki, Gunma, 370-1292, Japan*

[2]*Forschungszentrum Jülich GmbH, Jülich Centre for Neutron Science @ MLZ, Lichtenbergstraße 1, D-85747 Garching, Germany*

*To whom all correspondence should be addressed: Yue Zhao (zhao.yue@qst.go.jp); Yasunari Maekawa (maekawa.yasunari@qst.go.jp)

Unique Structural Characteristics of Graft-Type Proton Exchange Membranes using SANS Partial Scattering Function Analysis

Yue Zhao, Kimio Yoshimura, Shinichi Sawada, Toshinori Motegi, Akihiro Hiroki, Aurel Radulescu, Yasunari Maekawa

for Table of Contents use only

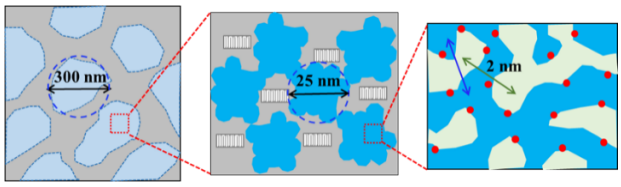

Abstract: The partial scattering function analysis was applied to determine the exact structure of radiation-grafted proton-exchange membranes, made of poly(styrenesulfonic acid)-grafted poly(ethylene-co-tetrafluoroethylene) (ETFE-g-PSSA). Hydrated ETFE-g-PSSA membranes were treated as a three-component system comprising ETFE base polymer (BP), PSSA graft polymer (GP), and absorbed water. On a large length scale, polymer grains with an approximate radius of gyration (R_g) of 150 nm and a mass fractal structure with a dimension of 2.4 were observed. These grains were formed by the aggregation of phase-separated GP domains in the BP matrix. Each individual GP domain has an average R_g of 9.5 nm and is composed of homogeneously distributed GP and water nanodomains that form a bicontinuous-like local structure with a mean separation distance of 2 nm. These structures were strongly supported by the first finding that PSSA GP and water interact attractively and repulsively in q-regions lower and higher than 2 nm^{-1} (*i.e.*, ~3 nm), respectively. The repulsion between GP and water at a molecular length level of <3 nm results in a lower hydration number and hence poorer conductivity at low relative humidity when compared to Nafion®. The results of this study provided a mechanistic insight into membrane conductivity and structure correlations.

I. Introduction

In polymer electrolyte fuel cells and other electrochemical applications, radiation-grafted membranes are an alternative to the state-of-the-art perfluorosulfonic acid polymer membranes, such as Nafion®.[1, 2] They offer the advantages of a potentially low-cost fabrication technique and the adaptability of polymer synthesis and functionalization, allowing easy modification of membrane properties by optimizing the materials (e.g., base polymer (BP), graft monomers, cross-linkers) and grafting parameters (e.g., grafting degree, crosslinking).[1–4] In general, the membrane properties must be carefully balanced to yield a satisfactory combination of proton conductivity, chemical stability, and mechanical integrity under dynamic operation conditions.

Due to its outstanding chemical, thermal, and mechanical stability, as well as its resistance to high-energy radiation, partially fluorinated poly(ethylene-co-tetrafluoroethylene) (ETFE) was recognized as an excellent base film for proton-exchange membrane (PEM) applying to salt production electrodialysis. Recently, the ETFE-based membranes has been also identified as a PEM for residential and automobile fuel cells.[5, 6] Various research groups have reported the fabrication of ETFE-based PEM by grafting styrene or its substitutes onto ETFE base films followed by sulfonation.[7–17] The resulting PEMs, such as poly(styrenesulfonic acid)-grafted ETFE (ETFE-g-PSSA) PEMs, were initially shown to have equivalent FC performance[8, 9] or even greater DMFC performance than Nafion®.[10, 11] Up to the current research stage, though drawbacks of ETFE-g-PSSA and their substituents membranes regarding the low proton conductivity under reduced relative humidity and the lack of long-term stability are still challenging and hinder their utilization in major fuel cell applications, the potential solutions have been approached by incorporating an adequate combination of monomers such as

glycidyl methacrylate,[14] acrylonitrile and methacrylonitrile,[15] crosslinking with divinylbenzene[16] and introducing HO-scavengers such as catechol-like compounds.[17] To overcome these shortcomings, one should take into account the balance between various physical, chemical and transport properties of these PEMs, which needs dedicated studies investigating the structure-property relationships.

When the PSSA-grafted PEMs are hydrated, the sulfonic acid (SA) groups absorb water and form hydrophilic ion-conducting nanodomains (ion channels) through which protons and water migrate, phase segregated from the hydrophobic polymer matrix. Thus, the proton conductivity and fuel cell performance are controlled by not only the density of the SA groups but also the morphology and connectivity of ion channels.[18] Small-angle X-ray scattering (SAXS) and neutron scattering (SANS) are the most potent techniques for investigating morphology in PSSA-grafted PEMs, such as crystalline structures and phase-separated hydrophobic/hydrophilic regions.[19–28] In conventional scattering analysis, the scattering intensity profile, $I(q)$, is plotted as a function of the scattering vector, q. The $I(q)$ profiles of these PEMs usually show two scattering characteristics: a broad peak in the low-q range at $0.1 < q < 0.3$ nm^{-1} (20–60 nm), corresponding to the microphase separation between graft polymer (GP) domains and base polymer (BP) matrix due to their immiscibility;[19–24] and a second peak in the high-q range at $1.5 < q < 3$ nm^{-1} (2–4 nm), so-called the "ionomer peak", associating with hydrophilic water domains and channels.[19, 21, 25–28] The structures of PEMs are usually obtained by the best fitting of appropriate structural models to their $I(q)$ profiles, for example, low-q peak is generally regarded as a distance characteristic determined by a complex combination of inter-domain distances, domain form, and effective interaction between adjacent domains.[19–24] However, the low-q peak related structures such as shape, size, and

chemical components of the origin are rarely studied, with the exception of a recent report by Narimani et al.,[21] where the hard-sphere fluid structure model (HS-fluid model) originally developed by Kinning and Thomas[29] was introduced to describe the morphology at low-q range for PEMs composed of a high content (at least 64% vol) of PS polymer chains grafted to poly-(vinylidene difuoride-*co*-chlorotrifluoroethylene) backbone. In comparison to the few analyses of the low-q peak, the high-q ionomer peak related structure has been thoroughly studied. There are primarily two proposed structural models: the Hard-Sphere-fluid model (HS-fluid model),[25, 26, 28] and the Teubner–Strey model (TS model).[21, 28] Both the HS-fluid and TS models represent isotropically and randomly distributed hydrophilic domains dispersed in a hydrophobic polymer matrix, with a mean separation distance closely related to the center position of the ionomer peak. The major difference between two models is the shape of domains: the HS-fluid model describes uniform spherical domains, whereas the TS model describes polydisperse and irregularly shaped domains. As previously described, both structural models adequately describe the ionomer peak associated with the water domains well.[21, 28]

The structure model is usually presumed to describe the typical structure pattern of a system without assigning components. Since the conventional $I(q)$ profile contains the scattering contributions from all the components and thus, scattering data used for a fitting procedure includes the mixed structural information of all components. This undesirable original data problem can be solved by analyzing the partial scattering function (PSF) profile of each component instead of $I(q)$ by using suitable structural model fitting. PSF profiles are the quantitative decomposition of a series of $I(q)$ obtained through the contrast variation SANS technique,[30–32] which was theoretically developed and applied to such as polymer nanocomposites,[32] but is yet barely known to PEM materials. Recently, we

developed PSF analysis in hydrated Nafion membranes, and successfully elucidate the concrete hierarchical structure of three-component domains of main-chain, side-chain, and water.[30] The primary advantage of PSF analysis over traditional scattering intensity analysis is that it allows for quantitative determination of the structure and location of each component in the membrane. Therefore, compared to the rough structure information (*i.e.*, the shape and size of scatters without component assignment) provided by intensity profiles, PSF profiles provide a deep understanding of precise structures with the exact location of each component in the material. In this study, for the first time, we applied the PSF analysis using suitable structural model fitting to visualize and quantify the detailed hierarchical structures of each component in hydrated ETFE-g-PSSA PEMs in multiple length scales and to provide structural insight in comparison to Nafion membranes.

II. Experimental details

II-1. Materials

The ETFE base film with a thickness of 50 μm (mass density = 1.75 g/cm^3, crystallinity (X_c) = 0.32) were purchased from Asahi Glass Co. Ltd, Japan. ETFE-g-PSSA membrane with a grafting degree (GD) of 38% and an ion exchange capacity of 2.0 mmol/g was prepared according to our previous report.[24, 33, 34] The crystallinity of the dried ETFE-g-PSSA membrane is 22% determined by DSC measurement.[33] The water uptake (WU) and swelling ratio (SR) of the fully hydrated membrane at room temperature were about 40% and 63.7%, respectively. Here, WU and SR are defined by the change of the membrane weight and volume between the dry and wet conditions, as $\mathrm{WU} = \frac{W_{wet}-W_{dry}}{W_{dry}} \times 100\%$, with W_{wet} and W_{dry} being the weight of the dry and wet membrane in

water, respectively; and $\mathrm{SR} = \frac{V_{wet} - V_{dry}}{V_{dry}} \times 100\%$, with V_{wet} and V_{dry} being the volume of the dry and wet membrane in water, respectively. The proton conductivity of the membrane was evaluated to be 0.104 S/cm at 60 °C in liquid water using electrochemical impedance spectroscopy. To ensure that the membranes were in the proton form, they were immersed in 1 M hydrochloric acid at room temperature for 1h and then washed with deionized water before the experiment. Fujifilm Wako Pure Chemical Co., supplied 1 M hydrochloric acid. Deionized water was purified by a Millipore Milli-Q UV system to produce water with a resistance of 18.2 MΩ·cm and a total organic carbon content of <10 ppb. Sigma-Aldrich Co. Ltd. supplied the deuterated water (D_2O, 99.9 atom% D) used in the SANS experiments.

II-2. Small-angle neutron scattering measurement

SANS measurements were performed on KWS-2 SANS diffractometer operated by Juelich Centre for Neutron Science at the neutron source Heinz Maier–Leibnitz (FRM II reactor) in Garching, Germany.[35] The incident neutron beam at KWS-2 was monochromatized with a velocity selector to have an average wavelength (λ) of 5 Å with a wavelength resolution of $\Delta\lambda/\lambda$= 20%. Before the SANS experiments, ETFE-g-PSSA membranes were equilibrated in water mixture with prescribed H_2O/D_2O ratio at room temperature for 24 h. The fully hydrated membranes were placed in SANS sample cells sealed by two quartz-plate windows with a silicon spacer in between to prevent evaporation, and then put on the neutron beam. All SANS measurements were performed at room temperature. The scattering patterns were collected using a two-dimensional (2D) scintillation detector and circularly averaged to obtain scattering intensity profiles as a function of q, where q is the scattering vector and defined as $q = (4\pi/\lambda)\sin(\theta/2)$, where θ is the scattering angle. The operable q-range in this study covers $0.03 < q < 5$ nm^{-1}. The

final intensity profiles obtained were corrected for the background of the cell, the electronic noise of the detector, detector sensitivity, and incoherent scattering.

II-3. Decomposition of scattering intensity profiles into Partial scattering functions

Following the strategy we applied to the hydrated Nafion membranes,[30] the fully hydrated ETFE-g-PSSA PEM is partitioned into separate components of ETFE (–$CH_2CH_2CF_2CF_2$–), graft polymer (–C_8H_7–SO_3H), and water as shown in Scheme 1.

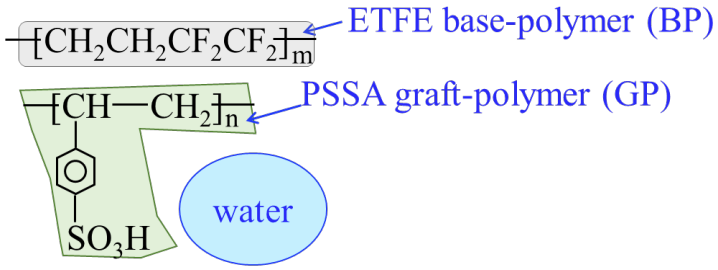

Scheme 1 An illustration of the three-component system of the fully hydrated ETFE-g-PSSA PEMs composed of ETFE base polymer (BP), PSSA graft polymer (GP) and water (W).

The quantitative decomposition of the scattering intensity profiles of a ternary system into PSFs has been detailed in the literature and S1 in the supporting information.[30–32, 36–39] On the basis of the incompressibility assumption, the scattering intensity profiles can be described by three PSF self-terms as follows.

$$I(q) = (b_{BP} - b_{GP})(b_{BP} - b_W)S_{BP-BP}(q) + (b_{GP} - b_{BP})(b_{GP} - b_W)S_{GP-GP}(q) + (b_W - b_{BP})(b_W - b_{GP})S_{W-W}(q) \quad (1)$$

where b_i and S_{ii} are the scattering length density (SLD) and PSF self-term of the i component (i = BP: ETFE base polymer, GP: PSSA graft polymer and W: water). S_{ii} is defined as

$$S_{ii}(q) = \frac{1}{V} < \iint \delta\varphi_i(\vec{\mathrm{r}})\delta\varphi_i\left(\vec{\mathrm{r}'}\right)\exp\left[-i\vec{q}\left(\vec{\mathrm{r}} - \vec{\mathrm{r}'}\right)\right]d\vec{\mathrm{r}}d\vec{\mathrm{r}'} > \qquad (2)$$

where V is the scattering volume and $\delta\varphi_i(\vec{\mathrm{r}})$ is the fluctuation part of the volume fraction of the *i* component at position $\vec{\mathrm{r}}$ ($\varphi_i(\vec{\mathrm{r}})$), which is expressed as

$$\delta\varphi_i(\vec{\mathrm{r}}) = \varphi_i(\vec{\mathrm{r}}) - \overline{\varphi_i} \qquad (3)$$

where $\overline{\varphi_i}$ is the average volume fraction of the *i* component (*i.e.*, $\overline{\varphi_i} = \frac{1}{V}\int \varphi_i(\vec{\mathrm{r}})d\vec{\mathrm{r}}$). The definition in Eq. (2) shows that $S_{ii}(q)$ is the Fourier transform of the autocorrelation function of $\delta\varphi_i(\vec{\mathrm{r}})$, $\gamma_i(\vec{\mathrm{u}})$, which is given by

$$\gamma_i(\vec{\mathrm{u}}) = \int \delta\varphi_i(\vec{\mathrm{r}})\delta\varphi_i(\vec{\mathrm{r}} + \vec{\mathrm{u}})d\vec{\mathrm{r}} \qquad (4)$$

As $\gamma_i(\vec{\mathrm{u}})$ specifies how $\delta\varphi_i(\vec{\mathrm{r}})$ and $\delta\varphi_i\left(\vec{\mathrm{r}'}\right)$ in neighboring regions separated by $\vec{\mathrm{u}}$ correlate with each other in real space, it gives the structural information of the *i* component.

When the SANS experiments are performed with *m* different contrast by using H_2O/D_2O mixtures, the obtained $I(q)$s (shown in Figure 1) are a group of linear equations of Eq (1), expressed as below

$$\begin{pmatrix} I_1(q) \\ \vdots \\ I_m(q) \end{pmatrix} = \boldsymbol{M} \cdot \begin{pmatrix} S_{BP-BP}(q) \\ S_{GP-GP}(q) \\ S_{W-W}(q) \end{pmatrix} \qquad (5)$$

where $\boldsymbol{M}$ is the coefficient matrix of the difference in SLD, as expressed below,

$$\boldsymbol{M} = \begin{pmatrix} {}^1\Delta_{BP-GP}\ {}^1\Delta_{BP-W} & {}^1\Delta_{GP-BP}\ {}^1\Delta_{GP-W} & {}^1\Delta_{W-BP}\ {}^1\Delta_{W-GP} \\ \vdots & \vdots & \vdots \\ {}^m\Delta_{BP-GP}\ {}^m\Delta_{BP-W} & {}^m\Delta_{GP-BP}\ {}^m\Delta_{GP-W} & {}^m\Delta_{W-BP}\ {}^m\Delta_{W-GP} \end{pmatrix} \qquad (6)$$

where ${}^m\Delta_{i-j} = {}^m\left(b_i - b_j\right)$ is the SLD difference between *i* and *j* in *m*th measurement. Thus, the three PSF self-terms of $S_{\mathrm{BP\text{-}BP}}(q)$, $S_{\mathrm{GP\text{-}GP}}(q)$ and $S_{\mathrm{W\text{-}W}}(q)$ on the right side of Eq. (5) can be mathematically determined through the series of $I(q)$ on the left side of Eq. (5).[30] The details can be found in S2 in the supporting information.

The PSF cross-term S_{ij} ($i \neq j$), defined by the following equation

$$S_{ij}(q) = \frac{1}{V} < \iint \delta\varphi_i(\vec{\mathrm{r}})\delta\varphi_j\left(\overrightarrow{\mathrm{r}'}\right)\exp\left[-i\vec{q}\left(\vec{\mathrm{r}} - \overrightarrow{\mathrm{r}'}\right)\right]d\vec{\mathrm{r}}d\overrightarrow{\mathrm{r}'} > \qquad (7)$$

can be deduced from S_{ii} using Eqs (8)–(10) under the incompressibility assumption.[30]

$$S_{BP-GP} = \frac{1}{2}(S_{W-W} - S_{BP-BP} - S_{GP-GP}) \qquad (8)$$

$$S_{GP-W} = \frac{1}{2}(S_{BP-BP} - S_{GP-GP} - S_{W-W}) \qquad (9)$$

$$S_{BP-W} = \frac{1}{2}(S_{GP-GP} - S_{BP-BP} - S_{W-W}) \qquad (10)$$

III. Results

III-1 Contrast variation SANS

Contrast variation SANS measurements were performed on ETFE-g-PSSA PEMs equilibrated in H_2O/D_2O mixtures with eight different volume fractions (f_{D2O}) of D_2O. The scattering intensity profiles, $I(q)$, for representative f_{D2O} are shown in Figure 1. In agreement with previously reported scattering profiles,[19–28] three typical features in the scattering profiles of ETFE-g-PSSA PEMs can be observed in specific three regions. Thus, we defined the corresponding regions in the figure as follows: A small-q upturn in the low-q region at $q < 0.12$ nm^{-1} (Region I), a broad shoulder-like scattering peak in the middle-q region at $0.12 < q < 1.5$ nm^{-1} (Region II), and a distinct scattering peak in the high-q region at $q > 1.5$ nm^{-1} (Region III).

In Region I, the scattering intensity decreases with increasing f_{D2O} and reaches a minimum at $f_{D2O} = 60\%$, then increases again at $f_{D2O} > 60\%$. The small-q upturn follows a power-law relationship with an exponent of about −2.4 for all profiles except for the case at $f_{D2O} = 60\%$ that has an exponent of −4. In Region II, except for the profile at $f_{D2O} = 60\%$, a broad peak appears at about $q_1 = 0.2$ nm^{-1}, and the corresponding d-spacing ($=2\pi/q_1$) is 31.4 nm. Similar to the change in Region I, the peak intensity decreases with

increasing f_{D2O} at $f_{D2O} < 60\%$ and then increases again at $f_{D2O} > 69\%$ without affecting the peak shape and width. The intensity profile reaches a minimum at $f_{D2O} = 60\%$ and the shoulder peak position shifts right to a higher q-range of $0.25 < q < 0.6$ nm^{-1}. Note that $I(q)$ profiles obtained through the contrast variation SANS technique vary based on hydrogen/deuterium replacement to change the scattering contrast, which is the difference in the SLD of the components in the system. In other words, the SLD of hydrophilic domains in the membrane is tuned by the absorbed water mixture of H_2O and D_2O, and consequently is the scattering contrast between the hydrophobic matrix and hydrophilic domains. Thus, the intensity change in Regions I and II indicates a fact that $f_{D2O} = 60\%$ is close to the point of contrast matching between the hydrophobic matrix and hydrophilic domains in the membrane. This contrast matching effect has been sufficiently discussed in section IV in conjunction with Figure 5. In Region III, the strong scattering peak appears at $q_2 = 2.7$ nm^{-1}, with a d-spacing ($=2\pi/q_2$) being 2.3 nm. Its intensity also first decreases and then increases as f_{D2O} increases, although at a different transition point approximately of $f_{D2O} = 40\%$, as clearly seen in the enlarged high-q plot in Figure S1 in the supporting information.

III-2. Partial scattering function analysis

If the system is composed of only two components, contrast variation experiments will change the absolute intensity but not the shape of the scattering profiles, according to Babinet's principle, which originally stated that the diffraction pattern from an opaque body is identical to that from a hole of the same size and shape.[30, 40] The supporting information in Ref. 30 has a detailed explanation for 2-component system. Therefore, the fully hydrated ETFE-g-PSSA PEM is not a simple "two-component" system, as shown in Figure 1. Because a structural analysis based just on $I(q)$ cannot quantitatively describe

the structure of each component in such a multiple-component system, we decompose the total scattering intensity profiles $I(q)$ into PSFs for each component.

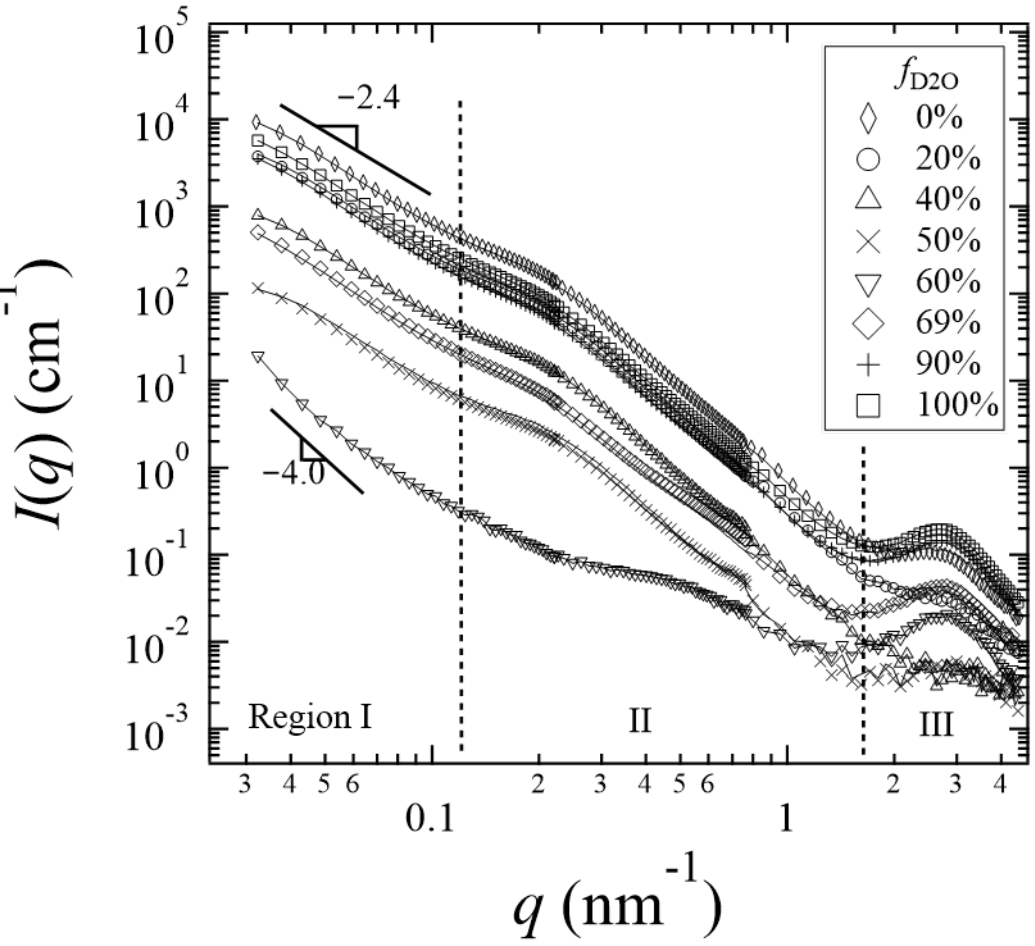

Figure 1 Experimental scattering intensity profiles (symbols) and the reconstructed intensity profiles (solid lines) of the fully hydrated ETFE-g-PSSA PEMs equilibrated in water mixtures of D_2O and H_2O with different ratios. The error bar of the data is within the symbols.

Following the method that we developed in the Nafion membrane,[30] we treat the hydrated ETFE-g-PSSA PEM consisting three components of ETFE BP, PSSA GP, and water, as shown in Scheme 1. The SLD of each component can be calculated using its

chemical structure and mass density.[41, 42] Theoretically derived SLDs for ETFE BP (b_{BP}) and PSSA GP (b_{GP}) are listed in Table 1. Water's SLD (b_W) varies as a function of the water mixture's f_{D2O}:

$$b_W = b_{D2O} f_{D2O} + b_{H2O}(1 - f_{D2O}) \qquad (11)$$

where b_{D2O} and b_{H2O} are the SLD of D_2O and H_2O being 6.34 and −0.56 ($\times 10^{10}$ cm^{-2}), respectively.[41, 42]

Table 1 SLD (b_x) of each component in the fully hydrated ETFE-g-PSSA PEMs.

Components	BP	GP	Water
b_x ($\times 10^{10}$ cm^{-2})	2.74	1.96	variable

With these well-defined SLD values, the self-term S_{ii} and cross-term S_{ij} ($i \neq j$) can be derived from Eq. (5) and Eqs. (8)–(10), respectively.[30] S_{ii} reflects the exact structure of the i component, whereas S_{ij} ($i \neq j$) contains information about the interaction between the i and j components and their relative positions. As a result, in the next sections we investigate the self-terms and cross-terms of PSFs independently.

Self-terms

The self-terms of three PSFs are shown as a function of q in Figure 2: ETFE BP (S_{BP-BP}), PSSA GP (S_{GP-GP}), and water (S_{W-W}). All SANS intensity profiles were reconstructed using Eq (5) via back-substitution with these three PSF self-terms. The reconstructed $I(q)$ profiles (solid lines) are well matched to the experimental profiles (symbols), as shown in Figure 1, indicating that S_{ii} with the appropriate SLDs is correct, *i.e.*, the PSF method is valid for ETFE-g-PSSA PEMs.

The absolute value of S_{ii} throughout the whole q range is $S_{BP-BP} > S_{W-W} > S_{GP-GP}$, as

shown in Figure 2. For S_{ii} is the Fourier transform of the autocorrelation function (γ_{ii}), as discussed in Section II-3 in conjunction with Eqs (2)–(4), this means that the real space magnitude of the autocorrelation functions for ETFE BP, water, and PSSA GP follow the same trend of $\gamma_{BP-BP} > \gamma_{W-W} > \gamma_{GP-GP}$. As a result, we can conclude that ETFE contributes more to the structural pattern than the other two components, meaning that ETFE acts as a template in the membrane.

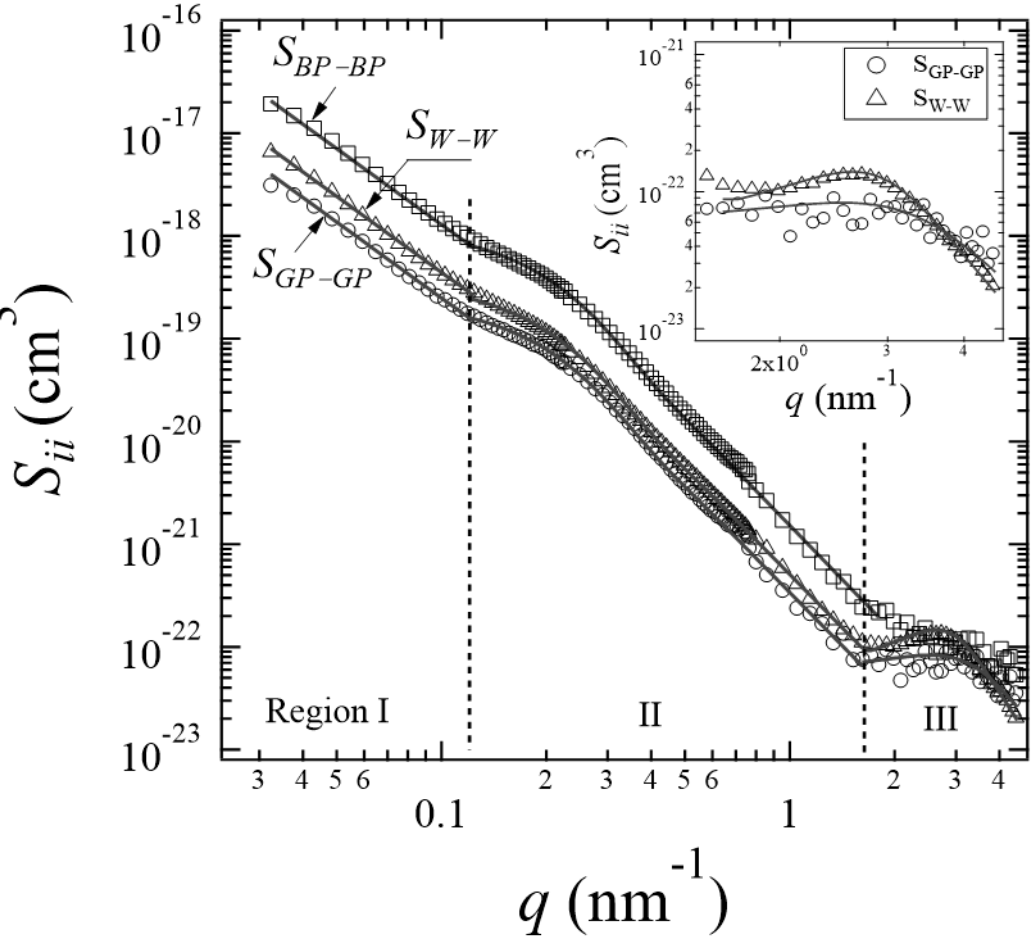

Figure 2 PSF self-terms of the fully hydrated ETFE-g-PSSA PEMs (symbols) and the best-fitted results obtained using Eq. (15) (solid lines). The inset shows the plots at $q > 1.5$ nm^{-1}. The fitting parameters are listed in Table 2.

The S_{ii} in Figure 2 shows several structural features in three q-regimes (Regions I, II, and III), as stated in Section 3.1. In Region I, all S_{ii} (*i.e.*, S_{BP-BP}, S_{GP-GP} and S_{W-W}) exhibits an upturn with a power-law exponent of about −2.4. In Region II, all S_{ii} shows a shoulder-like scattering maximum with a center position close to the peak observed in the scattering intensity profiles in Figure 1. In Region III, S_{GP-GP} and S_{W-W} show a peak with a center position close to the ionomer peak observed in the scattering intensity profiles, and S_{GP-GP} shows a comparatively broader peak than S_{W-W}, as shown in the inset of Figure 2. On the contrary, S_{BP-BP} in Region III is relatively flat and scattered, showing that the structure of ETFE is relatively homogeneous or structureless at this length scale.

Cross-terms

The PSF cross-terms S_{ij} ($i \neq j$) reflect cross-correlation between the components i and j. They are obtained in conjunction with S_{ii} through Eqs.(8)–(10). The sign of S_{ij} reveals the interaction force between i and j, with positive and negative values denoting attractive and repulsive interactions, respectively. The cross-terms of S_{BP-GP}, S_{BP-W}, and S_{GP-W} as a function of q are shown in Figure 3. S_{BP-GP} and S_{BP-W} are always negative with respect to q, whereas S_{GP-W} has the opposite sign at q values below and above 2 nm^{-1} (as shown in the inset of Figure 3), respectively.

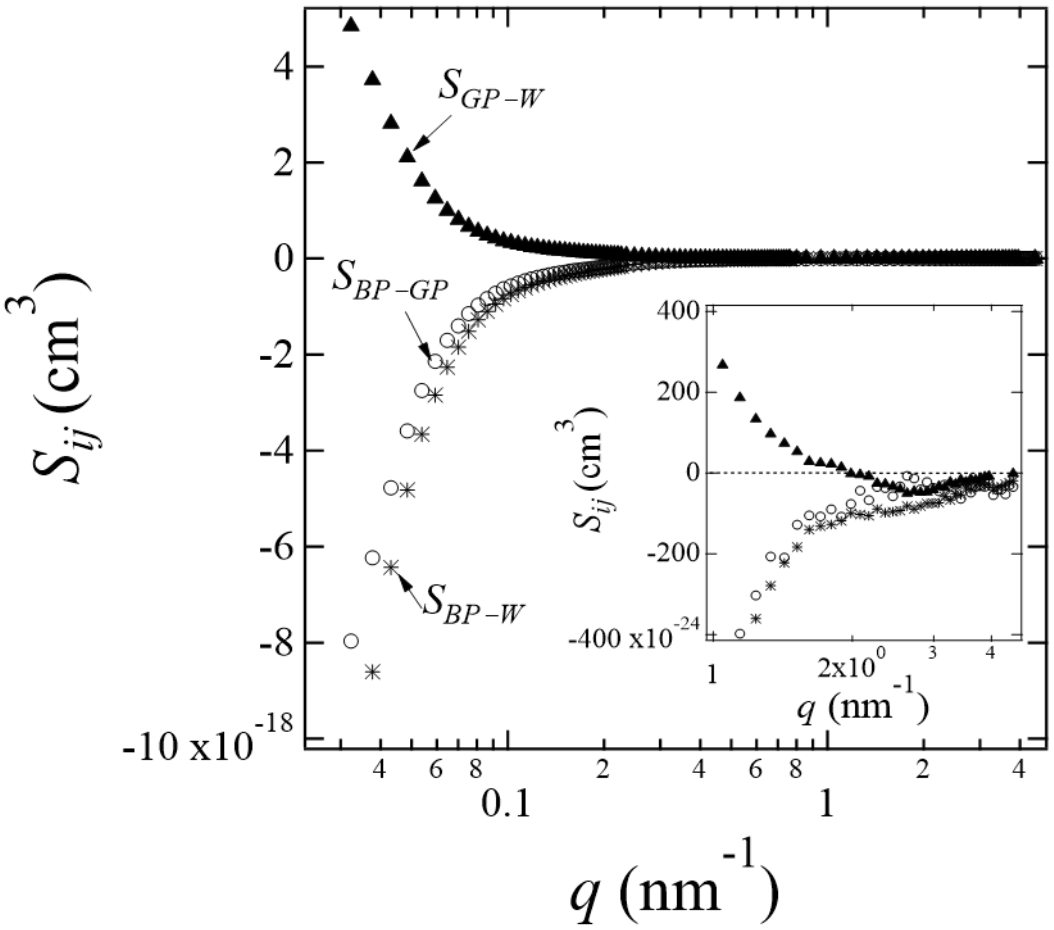

Figure 3 PSF cross-terms of the fully hydrated ETFE-g-PSSA PEMs. The inset shows the plots at $q > 1$ nm^{-1}.

III-3. Analysis on S_{ii} using structural models

As mentioned, S_{ii} reflects the concrete structure of the i component, including the arrangement and phase-separated morphology of BP, GP, and water in the membrane. In order to interpret S_{ii}, we use a fitting function with three main terms corresponding to different q-Regions, I, II, and III, individually. The features of each term are described below.

In Region I, S_{ii} shows a power-law dependence of q, which is a typical indicator of fractal structures of self-assembly of phase-separated domains in small-angle scattering

technique. The q range, in which scattering profiles obey a power-law dependence, is called the fractal region.[32, 43, 44] To evaluate the structure details, we apply the mass fractal (MF) structure model to fit the data in Region I as follows:

$$S_{MF}(q) \propto \frac{\Gamma(D_f-1)}{(1+q^2\xi^2)^{(D_f-1)/2}} \times \frac{\sin[(D_f-1)\tan^{-1}(q\xi)]}{q\xi} \qquad (12)$$

where $S_{MF}(q)$ is the MF function with the gamma function (Γ), MF dimension (D_f), and length of the upper cutoff of the MF structure (ξ).[32, 43, 44] In Eq. (12), ξ is defined as the upper cutoff radius of gyration of MF structures. In this study, we roughly estimate its value to be ~150 nm according to the shoulder-like peaks observed at $0.02 < q < 0.03$ nm^{-1} in ETFE-g-PSSA membranes using the Ultra-SAXS method reported by Tap *et al.*[24] Our choice of MF model function was partly motivated by the fact that BP is immiscible with GP. Therefore, one expects the microphase separation between BP and GP during the graft polymerization to cause the formation of small GP domains and, consequently, the large aggregates of GP domains. The aggregation process of individual GP domains is the origin of the MF structure. It should be noted that other model functions reported to fit the upturn in PEMs, such as the Debye-Bueche model (DB-model) describing scattering from random heterogeneities, did not provide an adequate fit to the data.[25, 28, 30]

In Region II, S_{ii} gives the shape of individual domains of the i component. The formation of the individual GP domains is random during the graft polymerization because GP domains are immiscible with BP and constrained by the BP matrix. Thus, it leads to the irregular shape of the GP domains. Accordingly, we employ the unified Guinier-exponential function (GE model), $S_{GE}(q)$, which is proposed to describe the irregular shape of individual domains. In particular, the GE model is an approximate form that describes a structure in scattering by Guinier's law and a power-law, generally being

reflected by a knee and a linear region on a log-log plot, respectively. These features are in good agreement with those of the S_{ii} profile in Region II. The GE model can closely duplicate structures for the irregularly shaped particles that display power-law behavior, as expressed below.[45-47]

$$S_{GE}(q) \propto \exp\left(\frac{-q^2 {R_g}^2}{3}\right) + B\left\{\frac{[\mathrm{erf}\left(\frac{kqR_g}{\sqrt{6}}\right)]^3}{q}\right\}^P \qquad (13)$$

where R_g is the particle's radius of gyration, erf(x) is the error function of x, and k is an empirical constant equal to 1.06.[45, 46] P ($3 < P < 4$) is the particle's surface fractal dimension as determined in the power-law region. B is a constant prefactor related to R_g and P by $B=P/{R_g}^P\Gamma(P/2)$.[45-47] We also tried using other models, such as the HS-fluid model[21, 28, 29] and the TS model,[21, 28, 30] and found that they less accurately fit the data comparing with the GE model.

For Region III, we chose a previously reported TS model that describes irregularly shaped bicontinuous domains with short-range order, to fit the peak in S_{GP-GP} and S_{W-W} profiles. The $S_{TS}(q)$ is the scattering function of the TS model expressed as below:[21, 28, 30, 48]

$$S_{TS}(q) \propto \frac{8\pi d^4}{\varepsilon[16\pi^4 + 8d^2\pi^2(\varepsilon^{-2} - q^2) + d^4(\varepsilon^{-2} + q^2)^2]} \qquad (14)$$

where d is the mean distance between two domains and determined from the peak position, q_m ($d = 2\pi/q_m$), and ε is considered as the dispersion of d (inversely proportional to the peak width). A broader peak leads to a smaller ε, indicating a more disordered bicontinuous structure with fewer interfacial correlations.[30, 48] Note that we also tried to use the HS-fluid model, which was also reported to fit the ionic peak in PEMs well, to fit the peak of S_{GP-GP} and S_{W-W} in Region III. However, we found the fits were not improved in comparison to the TS model, which is consistent with the previous report.[21, 28]

Considering the accuracy of the fitting model generally relies on the less use of fitting parameters, in this study we selected the TS model to describe the structure of each component in Region III.

With the addition of a constant background, the final fitting function is written as the sum of the three models:

$$S_{ii}(q) = C_1 S_{MF}(q) + C_2 S_{GE}(q) + C_3 S_{TS}(q) + C_B \qquad (15)$$

where C_1, C_2, and C_3 are the fitting constants, and C_B is the constant background.

The best-fitted curves obtained using Eq. (15) are shown together with S_{ii} in Figure 2. The fitting parameters, *i.e.*, D_f and ξ from the MF model, R_g and P from the GE model, and d and ε values from the TS model, are listed in Table 2.

Table 2 Best-fitting parameters in Eq (15) using MF, GE, and TS structural models

Models	MF model		GE model		TS model	
S_{ii}	ξ (nm)	D_f	R_g (nm)	P	d (nm)	ε (nm)
S_{BP-BP}	150±10	2.4±0.1	9.5±0.2	3.50±0.05	-	-
S_{GP-GP}	150±10	2.4±0.1	9.5±0.2	3.50±0.05	1.9±0.1	0.47±0.02
S_{W-W}	150±10	2.4±0.1	9.5±0.2	3.50±0.05	2.0±0.1	0.58±0.02

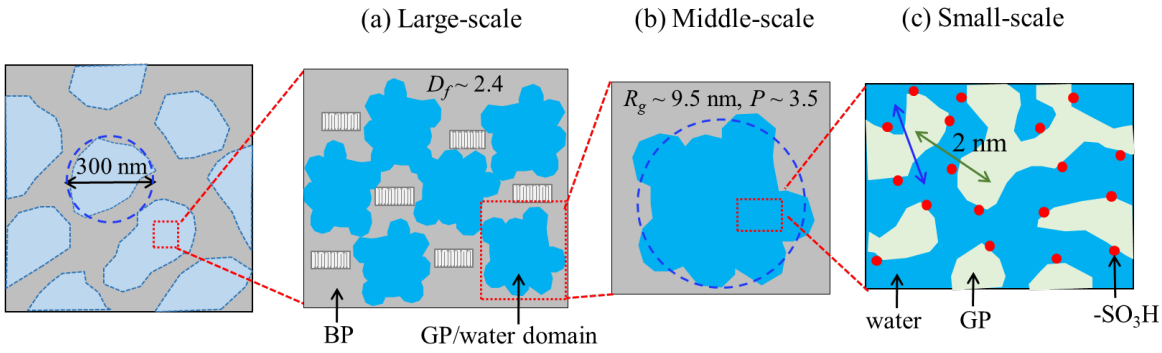

Figure 4 Schematic of the hierarchical structure of the ETFE base polymer, PSSA graft

polymer, and water domains in the fully hydrated ETFE-g-PSSA PEMs at (a) large-scale; (b) middle-scale; and (c) small-scale.

IV. Discussion

Three-component domains in the fully hydrated ETFE-g-PSSA PEM

Region I ($q < 0.12$ nm^{-1}).

A polymeric MF structure is made of self-similar polymer particles within a spatial range. When this range falls below a hundred nm, the scattering technique is the most appropriate way to study fractal structures and determine their fractal dimension, $D_{f,}$ in that the scattering law is given by q^{-Df}. D_f often summarizes complex structural details, such as polymer aggregates, which are generally related to the physical properties of the polymer materials.[49] The accurate determination of the fractal dimension associated with the cutoff size is given by the MF model using the scattering technique.[43, 44] In MF model analysis on S_{it} in Region I, the upper cutoff, ξ (=R_g of the domain, 150 nm), is assumed to be the characteristic size of the grain structure because the domain size is consistent with those observed by Ultra-SAXS results and the topographic image in atomic force microscopy (AFM).[24, 50] Mortensen *et al*. also reported similar shoulder-like peaks at the same q region in perfluorinated poly(ethylene propylene) based PSSA-grafted PEMs at the SANS instrument in National Institute of Standards and Technology (NIST).[22] The schematic picture of the large-scale structure is shown in Figure 4 (a).

Since the MF structures are not observed in the neat ETFE base film,[24, 51] we conclude that they originate from the aggregation of the small GP domains during the graft polymerization process, which are incorporated into but clearly phase-separate from the ETFE matrix, as evidenced by the repulsive interaction between GP and BP suggested

by the negative S_{BP-GP}. MF model analysis on S_{ii} in Region I indicates that all components show a similar mass fractal structure with a dimension of D_f = 2.4. In principle, D_f indicates how effectively the structure fills the available space. Smaller and larger values of D_f would imply more open and closed structures in the fractal objects. In other words, rather large D_f indicated that the aggregates were quite dense in structure. The value of the fractal dimension may also be useful for resolving the mechanism of cluster growth from the aggregation of small particles.[52] For instance, the D_f of polymer cluster aggregation was found to be 1.8 and 2.1 for diffusion-limited colloid aggregation and reaction-limited colloid aggregation (RLCA), respectively. The D_f of percolating networks exhibits a value as high as 2.5.[53] Therefore, here, D_f = 2.4 indicates the GP aggregates are more compactly packed by the individual GP domains than the usual RLCA mechanism during the polymerization, probably due to the BP matrix constraint sufficiently increasing the concentration of the GPs to form the aggregates. The incorporation of these GP domains in the ETFE matrix adds as MF structure to the BP matrix. Therefore, S_{BP-BP} shows the same MF structure feature as S_{GP-GP}. In addition, the positive S_{GP-W} and negative S_{BP-W} in Region I indicate that water is closely attached to the graft polymers due to the strong interaction with SA groups. Therefore, water domains must have coordinative movement with GP domains and form aggregates in the same way, which results in the same MF structure of water domains.

Region II ($0.12\ nm^{-1} < q < 1.5\ nm^{-1}$)**.**

In principle, the GE model describes two laws: Guinier's law and a power law, which give the average size of the structure unit and the surface or interfacial characteristics, respectively. The GE model analysis on S_{ii} in Region III shows all domains have a similar R_g of 9.5 nm, which is the average size of the individual building blocks for each

component to form the aggregates in Region I. The assignment of the individual domain size obtained by the GE model was supported by the consistent domain size observed in the phase image of AFM.[50] On one hand, PSSA GPs and water have coordinative movements, so the same size and distribution of graft polymer and water domains are expected; on the other hand, both graft polymers and water are phase-separated from ETFE, supported by the negative S_{BP-GP} and S_{BP-W}. Therefore, we reasonably conclude that water and graft polymers together form the homogeneous GP/water domains with a size of R_g = 9.5 nm. This specific R_g value is probably a result of two factors: (1) the minimization of the interfacial free energy between hydrophobic ETFE BP and hydrophilic PSSA graft polymers with water, and (2) the restriction of ETFE crystalline arrangement with a *d*-spacing of ~30 nm.[24, 51]

These coordinatively moved GP/water domains can be treated as one phase, which is distributed in the second phase ETFE matrix. Thus, the ETFE matrix exhibits the same structural pattern as the GP/water domains do according to the Babinet's principle.[40] Therefore, S_{BP-BP} is similar to both S_{GP-GP} and S_{W-W} in this q range. The power-law relationship in the high-q-regime in Region II allows for the estimation of P, which is ~3.5 for all components of BP, GP, and water. P is an indicative of the surface roughness of the domain, a smaller value than the typical sharp Porod surface (P = 4) indicates the surface of all the domains are not smooth. Based on the above discussion, a schematic of the structure in Region II is shown in Figure 4(b).

Another advantage of using the contrast variation SANS method is the ability to visualize the morphology of a material by contrast matching. It was mentioned in Figure 1 that the intensity profile at f_{D2O} = 60% shows dramatic deviations in comparison with other profiles, especially in Regions I and II, which originated from the contrast matching

effect. It is well accepted that polymer functional materials like PEMs are constructed by several phase separated structures at different structural levels (length scales or q-ranges), so-called "hierarchical structure". Given that a two-component case at a certain length scale, where components seen at other structural levels are negligible, the whole scattering intensity at this certain length scale can thus be cancelled at the contrast matching condition. This situation can be also confirmed by the fact that all the scattering profiles except that at the matching point, can be overlapped with one another at this certain q-range after normalizing by the contrast as we previously reported.[51] Thus, the contrast matching of the target components depends on the corresponding length scale. At the length scale in Regions I and II, BP domain and GP/water domain are visible components. At f_{D2O} = 60%, the SLD value of GP/water domain (= 2.95×10^{10} cm^{-2}) is close to that of crystalline ETFE chains (= 3.05×10^{10} cm^{-2}). Therefore, the contrast matching between BP and GP/water domains occurs, resulting in the elimination of the commonly observed shoulder-like scattering peak around 0.2 nm^{-1}, and making GP/water domains invisible. It is the invisible GP/water domains and the equivalent crystalline ETFE working together as a matrix that enables us to observe the detailed local structure of amorphous ETFE at the relative high-q range in Region II, and the crystalline/amorphous ETFE phase separation in Region I. Thus, at f_{D2O} = 60%, the crystalline ETFE and GP/water domains apparently behave as one component in Regions I and II. The other component is the amorphous ETFE domain with a SLD of 2.57×10^{10} cm^{-2}, which shows scattering contrast to the former component. Therefore, the hydrated ETFE-g-PSSA PEM at f_{D2O} = 60% can be treated as a 2-component system: the amorphous ETFE domains and the matrix composed of crystalline ETFE and GP/water domains.

The intensity profile of ETFE-g-PSSA PEMs at f_{D2O} = 60% was plotted in Figure 5. In the inset of the figure, we show the visible two components (amorphous ETFE chains in dark gray and the matrix in white) that make up the PEMs.

We have extensively discussed the relationship between $I(q)$ and $S_{ii}(q)$ for a typical two-component system previously,[30] and the key result is shown below:

$$I(q)_{fD2O=60\%} = (b_{am} - b_{mat})^2 S_{am-am}(q) = (b_{am} - b_{mat})^2 S_{mat-mat}(q) \quad (16)$$

where $I(q)_{fD2O=60\%}$ is the intensity profile of ETFE-g-PSSA PEMs at f_{D2O} = 60%, "am" and "mat" refer to the amorphous ETFE domains and the matrix containing the crystalline ETFE and hydrated domains, respectively. Eq. (16) shows that $I(q)_{fD2O=60\%}$ is proportional to $S_{am-am}(q)$ and thus represents the detailed structure of amorphous ETFE domains as well. The average size of amorphous ETFE domains (dark color in the inset of Figure 5) in Region II can be estimated by the unified GE function of Eq. (13). The Debye function, which we previously used to analyze the structure of amorphous ETFE domains in anion-exchange membranes, did not match the data in Region II well because of the obvious power-law deviation from –2 at $0.7 < q < 1.0$ nm^{-1}.[51] The best-fitting curve results in R_g = 3.0 nm and P = 3.3, corresponding to the typical size of the amorphous ETFE domain and the roughness of the domain surface, respectively, as shown in Figure 5. The power-law exponent of –4.0 in Regions I originated from the sharp boundary between crystalline and amorphous ETFE domains visible in the pristine ETFE base film.[24, 51]

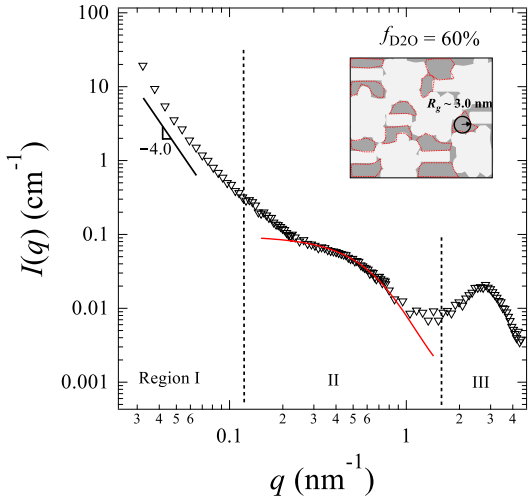

Figure 5 $I(q)$ profile of the hydrated ETFE-g-PSSA PEMs at f_{D2O} = 60% (symbols) and the best-fit curve using Eq. (13) (solid lines) in Region II. Inset: Schematic representation of the membrane structure at f_{D2O} = 60%, with dark gray amorphous ETFE domains and white matrix. R_g ~3.0 nm is shown in the figure for the individual amorphous domains surrounded by red dots.

Region III (q > 1.5 nm^{-1}).

The detailed local structure of the graft polymer and water in a GP/water domain can be explained in this region. The analysis of the S_{GP-GP} and S_{W-W} profiles by the TS model shows that both components have bicontinuous-like local structures with similar d values

(1.9–2.0 nm). S_{GP-W} showed a negative value in this region, despite showing a positive value in a lower q region < 2 nm^{-1}. Namely, the attractive and repulsive interactions between PSSA graft polymers and water are found at lower and higher q-regions than 2 nm^{-1} (*i.e.*, ~ 3 nm), which results in the homogeneous structure of GP and water in the hydrophilic domain with a size of 9.5 nm, but a bicontinuous-structure with a separation distance of 1.9 and 2.0 nm in the hydrophilic domain, respectively, as schematically shown in Figure 4(c). The main reason of the negative sign of S_{GP-W}, i.e., repulsive force between graft-polymers and water, should result from the immiscibility of hydrophobic styrene and water in the atomic scale (a few nm) in hydrophilic domains with about 10 nm channels.

However, the ε value of graft-polymer domains (~0.47 nm) is smaller than that of water domains (~0.58 nm), as shown by the broader peak of S_{GP-GP} in this region compared to S_{W-W}. Thus, the local structure of the GP domains is more disordered than that of the water domains, partly because the conformational relaxation and movement of a GP chain is slower than that of small molecules such as water, and partly because the confinement of GPs, which are chemically linked to the ETFE BP at one end and physically linked to water at the other end, makes the interface of the local GP domains more vague.

It is worthy to note that the PSF cross term of SA-containing side-chain and water in Nafion, S_{SC-W}, is always positive, even in the high-q range, showing that the interaction between Nafion side-chain and absorbed water is always attractive from microscopic to molecular levels.[30] This considerable difference of the interaction of polymer chains and water in Nafion and that in ETFE-g-PSSA PEMs should introduce fully phase-separated structure at whole q-range in Nafion, but not at polymer-water miscible hydrophilic

domains at approximately 10 nm scale in ETFE-g-PSSA PEMs. The fully phase-separated structure in Nafion results in a much higher hydration number (number of water molecules per SA, ~23) than that for ETFE-g-PSSA PEMs in this study (~11) under the fully hydrated condition. This difference might be the reason for the low swelling of ETFE-g-PSSA PEM under fully hydrated conditions, whereas lower conductivity under the low relative humidity (RH) conditions, as compared to Nafion.[33] This new finding is remarkably more advanced than the traditional structural analysis based on the scattering intensity profile, which specified only the information of ionomer peaks but not the accurate assignment of each component.[19–28] This study demonstrates for the first time the repulsive behavior between GP and water on a small length scale (molecular level) by the delicate PSF analysis using the contrast variation SANS technique. This structure factor is believed to affect the membrane conductivity significantly and requires special attention for the future PEM design.

V. Conclusions

We applied PSF analysis to gain quantitative knowledge of the role of each component in the entire structure of fully hydrated radiation-grafted ETFE-g-PSSA PEMs by contrast variation SANS experiments, which allow decomposition of the scattering intensity data into PSFs of each component.

Our results suggested three-component domains consisting of ETFE base polymer, PSSA graft polymers and water. PSF self-terms analysis revealed the detailed structure of each component, whereas the cross-terms gave the correlation between two components, leading to the location determination of the components. The entire structure patterns of the hydrated ETFE-g-PSSA PEMs were constructed in Figure 4. Polymer grains with a cutoff size of ~150 nm are formed by the aggregates of GP/water domains in a mass

fractal structure with a fractal dimension of 2.4 that are well phase-separated and dispersed in the ETFE BP matrix. Each GP/water domain is made of homogeneously incorporated GP and water with an average size of R_g = 9.5 nm. In each GP/water domain, both GP and water show a bicontinuous-like local structure, showing the formation of a well-connected ion channel network, a key structural factor for high membrane conductivity that was found in Nafion membranes.[30, 54-56] Additionally, our PSF cross-term analysis shows that GP and water are repulsive at the molecular length level <3 nm, resulting in a lower hydration number and hence a lower conductivity at low RH compared to Nafion membranes.

Note that the conductivity of fuel cells at low RH is of great scientific interest. This study shows that PSF analysis is capable of providing mechanistic insights concerning structural correlations over a range of length scales, from microscopic to molecular. In particular, the structural guidelines at the molecular level are significant and relevant for establishing superior design rules for fuel cell membranes.

Notes

The authors declare no competing financial interest.

Acknowledgments

This work was partially supported by Grant-in-Aid for Scientific Research (A) from Japan Society for the Promotion of Science (JSPS) (KAKENHI Grant Number: 18H03850), and partially supported by "Advanced functional polymer materials alliance" project under QST innovation hub program in collaboration with participant companies, and "FY2021 Diversity Promotion Collaborative Research Subsidy" by the Diversity Promotion Office in QST.

Supporting information

Incompressibility assumption for a ternary system; Decomposition of scattering intensity profiles into partial scattering functions by contrast variation SANS; The scattering intensity profiles in Region III for fully hydrated ETFE-g-PSSA PEMs equilibrated in water mixtures of D_2O and H_2O with different ratios

References.

1. Nasef, M. M. Radiation-grafted membranes for polymer electrolyte fuel cells: current trend and future directions, *Chem. Rev.* **2014**, *114*, 12278-12329.
2. Nasef, M. M.; Gürsel, S. A.; Karabelli, D.; Güven, O. Radiation-grafted materials for energy conversion and energy storage applications, *Progr. Polym. Sci.* **2016**, *63*, 1-41.
3. Nasef, M. M.; Güven, O. Radiation-grafted copolymers for separation and purification purposes: Status, challenges and future directions, *Progr. Polym. Sci.* **2012**, *37*, 1597-1656.
4. Gubler, L.; Bonorand, L. Radiation grafted membranes for fuel cells: strategies to compete with PFSA membranes, ECS trans. **2013**, *58*, 149-162.
5. Gubler, L. Polymer design strategies for radiation-grafted fuel cell membranes, *Adv. Energy Mater.* **2014**, *4*, 1300827.
6. Nasef, M. M., Saidi, H.; Dahlan, K. Z. M. Electron beam irradiation effects on ethylene-tetrafluoroethylene copolymer films, *Radiat. Phys. Chem.* **2003**, *68*, 875-883.
7. Brack, H. P.; Bührer, H. G.; Bonorand, L., Scherer, G. G. Grafting of pre-irradiated poly(ethylene-alt-tetrafluoroethylene) films with styrene: influence of base polymer film properties and processing parameters, *J. Mater. Chem.* **2000**, *10*, 1795-1803.

8. Horsfall, J. A.; Lovell, K. V. Synthesis and characterisation of sulfonic acid-containing ion-exchange membranes based on hydrocarbon and fluorocarbon polymers, *Eur. Polm. J.* **2002**, *38*, 1671-1682.
9. Horsfall, J. A.; Lovell, K. V. Performance of Radiation Grafted Sulphonic Acid Membranes, *Fuel Cells* **2001**, *1*, 186-191.
10. Scott, K.; Taama, W. M.; Argyropoulos, P. Performance of the direct methanol fuel cell with radiation-grafted polymer membranes, *J. Membr. Sci.* **2000**, *171*, 119-130.
11. Aricò, A.; Baglio, V.; Creti, P.; Di blasi, A.; Antonucci, V.; Brunea, J.; Chapotot, A.; Bozzi, A.; Schoemans, J. Investigation of grafted ETFE-based polymer membranes as alternative electrolyte for direct methanol fuel cells, *J. Power Sources* **2003**, *123*, 107-115.
12. Chen, J.; Asano, M.; Maekawa, Y.; Yoshida, M. Suitability of some fluoropolymers used as base films for preparation of polymer electrolyte fuel cell membranes, *J. Membr. Sci.* **2006**, *277*, 249-257.
13. Chen, J.; Asano, M.; Maekawa, Y.; Yoshida, M. Polymer electrolyte hybrid membranes prepared by radiation grafting of *p*-styryltrimethoxysilane into poly(ethylene-*co*-tetrafluoroethylene) films, *J. Membr. Sci.* **2007**, *296*, 77-82..
14. Sproll, V.; Schmidt, T. J.; Gubler, L. Effect of glycidyl methacrylate (GMA) incorporation on water uptake and conductivity of proton exchange membranes, *Radiat. Phys. Chem.* **2018**, *144*, 276-279.
15. Gubler, L.; Slaski, M.; Wokaun, A.; Scherer, G. G. Advanced monomer combinations for radiation grafted fuel cell membranes, *Electrochem. Commun.* **2006**, *8*, 1215-1219.
16. Li. J.; Muto, F.; Miura, T.; Oshima, A.; Washio, M.; Ikeda, S.; Iida, M.; Tabata, Y.; Matsuura, C.; Katsumura, Y. Improving the properties of the proton exchange

membranes by introducing α-methylstyrene in the pre-irradiation induced graft polymerization, *Eur. Polym. J.* **2006**, *42*, 1222-1228.

17. Dockheer, S. M.; Gubler, L.; Bounds, P. L.; Domazou, A. S.; Scherer, G. G.; Wokaun, A.; Koppenol, W. H. Damage to fuelcell membranes reaction of HO· with an oligomer of poly(sodium styrene sulfonate) and subsequent reaction with O_2, *Phys. Chem. Chem. Phys.* **2010**, *12*, 11609-11616.
18. Gürsel, S. A.; Gubler, L.; Gupta, B.; Scherer G. G. In *Fuel Cells I*; Abe, A.; Albertsson, A. C.; Duncan, R.; Dusek, K. Eds.; Springer: Berlin, Heidelberg, 2008; Vol. 215.
19. Nagy, G.; Sproll, V.; Gasser, U.; Schmidt, T. J.; Gubler, L.; Balog, S. Scaling the graft length and graft density of irradiation-grafted copolymers, *Macromol. Chem. Phys.* **2018**, *219*, 1800311.
20. Sproll, V.; Nagy, G.; Gasser, U.; Embs, J. P.; Obiols-Rabasa, M.; Schmidt, T. J.; Gubler, L.; Balog, S. Radiation grafted ion-conducting membranes: the influence of variations in base film nanostructure, *Macromolecules* **2016**, *49*, 4253-4264.
21. Narimani, R.; Yang, A. C. C.; Tsang, E. M. W.; Rubatat, L.; Holdcroft, S.; Frisken, B. J. Controlling water content and proton conductivity through copolymer morphology, *Macromolecules* **2013**, *46*, 9676-9687.
22. Mortensen, K.; Gasser, U.; Gürsel, S. A.; Scherer G. G. Structural characterization of radiation-grafted block copolymer films, using SANS technique, *J. Polym. Sci: Part B: Polym. Phys.* **2008**, *46*, 1660-1668.
23. Song, J. M.; Ko, B. S.; Sohn, J. Y.; Nho, Y. C.; Shin, J. A study on the morphology of polystyrene-grafted poly(ethylene-alt-tetrafluoethylene) (ETFE) films prepared using a simultaneous radiation grafting method, *Radiat. Phys. Chem.* **2014**, *97*, 374-380.
24. Tap, T. D.; Sawada, S.; Hasegawa, S.; Yoshimura, K.; Oba, Y.; Ohnuma, M.;

Katsumura, Y.; Maekawa, Y. Hierarchical structure-property relationships in graft-type fluorinated polymer electrolyte membranes using small- and ultrasmall-angle X-ray scattering analysis, *Macromolecules* **2014**, *47*, 2373-2383.

25. Balog, S.; Gasser, U.; Mortensen, K.; Ben youcef, H.; Gubler, L.; Scherer, G. G. Structure of the ion-rich phase in DVB crosslinked graft-copolymer proton-exchange membranes, *Polymer* **2012**, *53*, 175-182.
26. Balog, S.; Gasser, U.; Jetsrisuparb, K.; Gubler, L. Structure of the hydrophilic phase and its impact on the conductivity of graft copolymer ionomers at low hydration level, *Polymer* **2013**, *54*, 4266-4275.
27. Balog, S.; Jetsrisuparb, K.; Gasser, U.; Scherer, G. G.; Gubler, L. Structure of the aqueous phase and its impact on the conductivity of graft copolymer ionomers at saturation, *Polymer* **2014**, *55*, 3026-3036.
28. Balog, S.; Gasser, U.; Mortensen, K.; Ben youcef, H.; Gubler, L.; Scherer, G. G. Nano-scale morphology in graft copolymer proton-exchange membranes cross-linked with DIPB, *J. Membr. Sci.* **2011**, *383*, 50-59.
29. Kinning, D. J.; Thomas, E. L., Hard-sphere interactions between spherical domains in diblock copolymer, *Macromolecules* **1984**, *17*, 1712− 1718.
30. Zhao, Y.; Yoshimura, K.; Motegi, T.; Hiroki, A.; Radulescu, A.; Maekawa, Y. Three-component domains in the fully hydrated Nafion membrane characterized by partial scattering function analysis, *Macromolecules* **2021**, *54*, 4128-4135.
31. Shibayama, M. Chapter 8 Soft Condensed Matter, *Experimental Methods in the Physical Sciences, Neutron Scattering-applications in biology, chemistry and materials science,* edited by Fernandez-Alonso, F. and Price D. L., **2017**, *46*, 459-546.

32. Endo, H.; Schwahn, D.; Colfen, H. On the role of block copolymer additives for calcium carbonate crystallization: small angle neutron scattering investigation by applying contrast variation, *J. Chem. Phys.* **2004**, *120*, 9410-9423.
33. Tap, T. D.; Sawada, S.; Hasegawa, S.; Katsumura, Y.; Maekawa, Y. Poly(ethylene-co-tetrafluoroethylene) (ETFE)-based graft-type polymer electrolyte membranes with different ion exchange capacities: relative humidity dependence for fuel cell applications, *J. Membr. Sci.* **2013**, *447*, 19-25.
34. Sawada, S.; Hasegawa, S.; Zhao, Y.; Maekawa, Y. block-type proton exchange membranes prepared by a combination of radiation-induced grafting and atom-transfer radical polymerization, *J. Membr. Sci.* **2017**, *532*, 105-114.
35. Radulescu, A.; Pipich, V.; Frielinghaus, H.; Appavou, M. S. KWS-2, the high intensity / wide Q -range smallangle neutron diffractometer for soft-matter and biology at FRM II, *Journal of Physics: Conference Series* **2012**, *351*, 012026.
36. Endo, H.; Miyazaki, S.; Haraguchi, K.; Shibayama, M. Structure of nanocomposite hydrogel investigated by means of contrast variation small-angle neutron scattering, *Macromolecules* **2008**, *41*, 5406-5411.
37. Matsunaga, T.; Endo, H.; Takeda, M., Shibayama, M. Microscopic structure analysis of clay-poly(ethylene oxide) mixed solution in a flow field by contrast-variation small angle neutron scattering, *Macromolecules* **2010**, *43*, 5075-5082.
38. Takanaka, M.; Nishitsuji, S.; Amino, N.; Ishikawa, Y.; Yamaguchi, D.; Koizumi, S. Structure analyses of swollen rubber-filler systems by using contrast variation SANS, *Macromolecules* **2009**, *42*, 308-311.
39. Noda, Y.; Koizumi, S.; Masui, T.; Mashita, R.; Kishimoto, H.; Yamaguchi, D.; Kumada, T.; Takata, S.; Ohishi, K.; Suzuki, J. Contrast variation by dynamic nuclear

polarization and time-of-flight small-angle neutron scattering. I. Application to industrial multi-component nanocomposites, *J. Appl. Cryst.* **2016**, *49*, 2036-2045.

40. Born, M.; Wolf, E. *Principles of Optics*; Cambridge University Press: Cambridge, 1999.
41. See for example, Roe, R. J. *Methods of X-ray and neutron scattering in polymer science*; Oxford Uni. Press: New York, 2000.
42. SLD of a component with molecules composed of *i* atoms, can be calculated from the expression given by $SLD = (\frac{dN_A}{M_w}) \sum_i b_i$, where b_i is the scattering length of *i*th atom, d is the mass density of the component, M_w is the molecular weight, and N_A is the Avogadoro constant. The mass densities of ETFE backbone and SO_3H are supposed to be 1.7 (Sigma-Aldrich) and 2.3 (ChemSpider) g/cm^3, respectively. Thus the mass density of graft-chain (C_8H_7-SO_3H) is calculated to be 1.38 g/cm^3, in terms of the mass density of polystyrene part in the graft-chain being 1.05 g/cm^3. SLD of a component can be estimated with the knowledge of abovementioned mass density and its molecular structure.
43. Sinha, S. K.; Freltoft, T.; Kjems, J. in *Kinetics of Aggregation and Gelation*; Family, F.; Landau D. P. Eds.; Elsevier: Amsterdam, 1984.
44. Freltoft, T.; Kjems, J.; Sinha, S. K. Power-law correlations and finite-size effects in silica particle aggregates studied by small-angle neutron scattering, *Phys. Rev. B* **1986**, *33*, 269-275.
45. Izawa, K.; Ogasawara, T.; Masuda, H.; Okabayashi, H.; Monkenbusch, M.; O'Connor, C. J. Growth process for fractal polymer aggregates formed by perfluorooctyltriethoxysilane. Time-resolved small-angle X-ray scattering spectra and the application of the unified equation, *Colloid Polym Sci* **2002**, *280*, 725–735.

46. Beaucage, G. Small-Angle Scattering from Polymeric Mass Fractals of Arbitrary Mass-Fractal Dimension, *J. Appl. Crystallogr.* **1996**, *29*, 134-146.

47. Beaucage, G.; Schaefer, D. W. Structural studies of complex systems using small-angle scattering: a unified Guinier/power-law approach, *J. Non-Cryst. Solids* **1994**, *172–174*, 797-805.

48. Teubner, M.; Strey, R. Origin of the scattering peak in microemulsions, *J. Chem. Phys.* **1987**, *87*, 3195-3200.

49. Witten, T. A.; Sander, L.M. Diffusion-limited aggregation, *Phys. Rev. B* **1983**, *27*, 5686-5697.

50. Motegi, T.; Yoshimura, K.; Zhao, Y.; Hiroki, A.; Maekawa, Y. Direct Observation and Semiquantitative Analysis of Hierarchical Structures in Graft-type Polymer Electrolyte Membranes using AFM Technique, *Langmuir* submitted.

51. Zhao, Y.; Yoshimura, K.; Shishitani, H.; Yamaguchi, S.; Tanaka, H.; Koizumi, S.; Szekely, N.; Radulescu, A.; Richter, D.; Maekawa, Y. Imidazolium-based anion exchange membranes for alkaline anion fuel cells: elucidation of the morphology and the interplay between morphology and properties, *Soft Matter* **2016**, *12*, 1567-1578.

52. Lin, M. Y.; Lindsay, H. M.; Weitz, D. A.; Ball, R. C.; Klein, R. Universality in colloid aggregation, *Nature*, **1989**, *339*, 360-362.

53. Li, Y. C.; Chen, K. B.; Chen, H. L.; Hsu, C. S.; Tsao, C. S.; Chen, J. H.; Chen, S. A. Fractal Aggregates of Conjugated Polymer in Solution State, *Langmuir* **2006**, *22*, 11009-11015.

54. Allen, F. I.; Comolli, L. R.; Kesoglu, A.; Modestino, M. A.; Minor, A. M.; Weber, A. Z. Morphology of hydrated as-cast Nafion revealed through Cryo electron tomography, *ACS Macro Lett.* **2015**, *4*, 1-5.

55. Elliott, J. A.; Wu, D. S.; Paddison, S. J.; Moore, R. B. A unified morphological description of Nafion membranes from SAXS and mesoscale simulations, *Soft Matter* **2011**, *7*, 6820-6827.

56. Sugiyama, M.; Mitsui, T.; Sato, T.; Akai, Y.; Soejima, Y.; Orihara, H.; Na, Y. H.; Itoh, K.; Mori, K.; Fukunaga, T. Structural analysis of polyelectrolyte film absorbing metal ion by SAXS utilizing with X-ray anomalous dispersion effect, *J. Phys. Chem. B* **2007**, *111*, 8663-8667.